Resonances in the Photo-Ionization Continuum of Ne I (20–150 eV)*

K. CODLING, R. P. MADDEN, AND D. L. EDERER
National Bureau of Standards, Washington, D. C.
(Received 23 September, 1966)

The absorption spectrum of neon in the region 20–150 eV has been studied photographically and photoelectrically, using synchrotron light as a background source. Discrete structure has been observed in three distinct energy ranges. The first is between the $^2P^\circ_{1/2,\,3/2}$ limits near 22 eV, involving resonances analogous to those observed by Beutler in Ar, Kr, and Xe; the second is the region between 44 and 60 eV, the structure here being classified as due to two types of excitation: (i) the excitation of a subshell $2s$ electron, (ii) the simultaneous excitation of two outer $2p$ electrons; the third region is near 80 eV, where two weak resonances are observed, due to the simultaneous excitation of a subshell $2s$ and a $2p$ electron. The resonance profiles of the states $2s\,2p^6\,np\,{}^1P^\circ_1$, where $n=3$, 4, and 5, and the two-electron excitation state $2p^4\,(^3P)\,3s\,3p\,{}^1P^\circ_1$ have been studied quantitatively and values of q, Γ, and ρ determined for each.

I. INTRODUCTION

THE discovery of discrete structure in the photo-ionization continuum of Ne I due to auto-ionizing states was reported in an earlier paper.[1] In that preliminary report, prominent resonances in the continuous absorption cross section were identified as due to the excitation of an inner subshell electron, $2s^2\,2p^6\,{}^1S_0 \rightarrow 2s\,2p^6\,np\,{}^1P_1^\circ$. The presence of other resonances in the 200–300 Å region and their probable association with optically allowed two-electron excitations in neon were also mentioned. Some of the present quantitative results have been previously communicated to theoretical workers.[2,3]

The most prominent of the optically observed resonances have since been seen by other techniques, as reported by Simpson *et al.*[4] in the study of the energy of electrons scattered by neon, and more recently by Rudd and Lang[5] who analyzed the energy of electrons ejected from neon when bombarded by protons and H_2^+ particles. These studies of neon resonances in particle scattering are to a large extent complementary to the photon experiments, since many of the resonances found are due to states which cannot be reached by optical absorption from the ground state. However, the understanding of the optically observed resonances obtained with good resolution and high accuracy, is a necessary prerequisite to the analysis of the more complex and less well-resolved spectra obtained in the particle-scattering experiments.

This paper summarizes our extended observations on auto-ionizing states in neutral neon, and presents an analysis of the spectrum as completely as is possible without further accurate calculations of the energies of two-electron excitation states in neon. It is generally difficult to predict these energies, since the electron core is left with an unfilled outer shell and the two excited electrons screen one another. It is also found that the two-electron excitation configurations interact with each other, as well as with the underlying continua. As a result of these prediction difficulties, and also because of the breadth and weak contrast of some of the resonances, the identifications suggested below are not all equally reliable.

In addition to the energies of the observed resonances, the absorption profiles of the more prominent ones have been studied, resulting in the experimental determination of the profile parameters (q, Γ, and ρ) for these resonances.

While the discrete structure in neon above its ionization limit (21.56 eV) has not been studied previously, the shape of the continuous background absorption has been carefully studied[6,7] and is now rather well established. Hence, this paper will be concerned only with the discrete structure which has been found superimposed on this continuous background. The shapes of the resonances which occur therein vary considerably. Many appear as absorption lines superimposed on the background continuum, while others are asymmetric, having a reduced absorption or "window" zone just to the high-energy side of an enhanced absorption zone. All of the resonance shapes observed, however, can be fitted by the generalized "Beutler-Fano" profile as recently formulated by Fano and Cooper.[2]

The absorption measurements were made possible by utilizing the NBS 180-MeV electron synchrotron as a background light source.[8] The continuum radiated by the orbiting electrons in this machine has been similarly used to investigate discrete auto-ionizing structure in the photo-ionization continua of the other rare gases.[9,10]

* This work was supported in part by the U. S. Atomic Energy Commission.
[1] R. P. Madden and K. Codling, Phys. Rev. Letters **10**, 516 (1963).
[2] U. Fano and J. W. Cooper, Phys. Rev. **137**, A1364 (1965).
[3] K. Sewell, J. Opt. Soc. Am. **55**, 739 (1965).
[4] J. A. Simpson, S. R. Mielczarek, and J. W. Cooper, J. Opt. Soc. Am. **54**, 269 (1964).
[5] M. E. Rudd and D. Lang, in *Proceedings of the Fourth International Conference on Physics of Electronic and Atomic Collisions, Quebec, 1965*, edited by L. Kerwin and W. Fite (Science Bookcrafters, Hastings-on-Hudson, New York, 1965), p. 153.
[6] D. L. Ederer and D. H. Tomboulian, Phys. Rev. **133**, A1525 (1964).
[7] J. A. R. Samson, J. Opt. Soc. Am. **55**, 935 (1965).
[8] K. Codling and R. P. Madden, J. Appl. Phys. **36**, 380 (1965).
[9] R. P. Madden and K. Codling, J. Opt. Soc. Am. **54**, 268 (1964).
[10] K. Codling and R. P. Madden, Phys. Rev. Letters **12**, 106 (1964).

An analysis of the two-electron excitation states found in helium has been published.[11] The present paper is intended, therefore, as the second of a series of articles covering our observations of these high-lying states in the rare gases.

II. EXPERIMENTAL DETAILS

The spectra were photographed with a 3-m grazing-incidence spectrograph, and the resonance profiles were obtained using a photoelectric scanning 3-m grazing-incidence monochromator. Both of these instruments were designed and constructed specifically for use with the NBS 180 MeV electron synchrotron, where vibration and temperature variation are two serious problems. In these experiments the spectral resolution of either instrument was about 0.06 Å. Eastman SWR plates were used in the spectrograph and a Bendix magnetic multiplier was the detector in the monochromator. Figure 1 indicates the general experimental arrangement of the instruments in place on the synchrotron. Additional details of the spectrograph and monochromator will be given elsewhere.[12] Both instruments utilize 600 lines/mm gratings at an angle of incidence of 84.5°. These instruments have been designed so that inactive gases can be studied in absorption by placing them directly in the spectrometers. Thus, in these experiments, no auxiliary absorption cell was used. The absorption path was the total optical path between entrance and exit slits. With the aid of differential pumping, a pressure of approximately 0.2 Torr could be maintained in the spectrometers, while the synchrotron vacuum system was held below 10^{-5} Torr. The monochromator also required additional pumping on the detector side of the exit slit to maintain the magnetic multiplier in an environment below 10^{-5} Torr.

The neon used for these measurements was high-purity commercial neon (99.995% pure). The optical

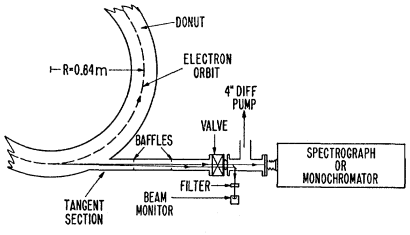

FIG. 1. Experimental arrangement for utilizing "synchrotron light" for absorption studies. The light emitted along the electron orbit tangent is incident upon the entrance slit of either the 3-m grazing incidence spectrograph or monochromator (600l/mm grating, 84.5° of incidence). Foil filters (not shown) may be inserted between synchrotron and entrance slit for order separation. The gas absorption path is the optical path of the spectrometer.

[11] R. P. Madden and K. Codling, Astrophys. J. **141**, 364 (1965).
[12] R. P. Madden, D. L. Ederer, and K. Codling, Appl. Opt. **6**, 31 (1967).

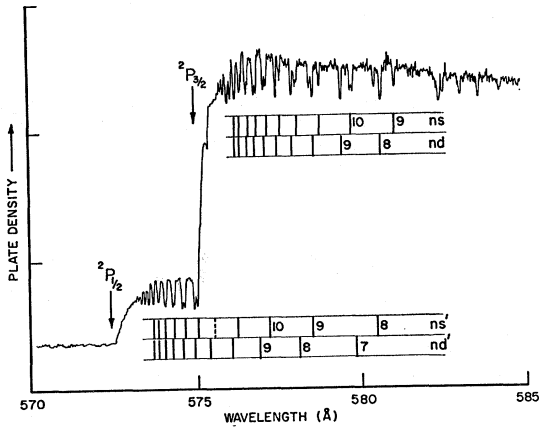

FIG. 2. A densitometer trace of the absorption spectrum of Ne I observed photographically in the 570–585 Å region, showing the resonances between the lowest $^2P_{1/2}{}^\circ$ and $^2P_{3/2}{}^\circ$ terms of Ne II.

absorption paths range from 60 to 120 cm and the pressures from 0.01 to 0.20 Torr as determined by a McLeod gauge.

The monochromator detector was operated as a counter, with typically 100 to 200 counts/sec. The counting rate was recorded in ratio to the visible light signal from the synchrotron as measured by another photomultiplier. Thus, fluctuations in the synchrotron light due to variation in the electron capture efficiency of the synchrotron were greatly reduced. Many scans over the resonances were made to improve the signal-to-noise ratio in the averaged results. The slit widths of the monochromator were accurately known, namely 11 ± 1 μ. Thus it was possible to calculate the effect of smearing the resonance profiles by the instrumental slit function.

III. SPECTRA

The absorption of neutral neon has been photographically recorded from 80–600 Å, i.e., from 1 eV below the lowest ionization limit (21.56 eV) to about 135 eV above. Over this range, discrete structure was found in three spectral regions, superimposed upon the continuous absorption. The first is between the $2p^5\,{}^2P^\circ_{1/2,3/2}$ limits, as shown in Fig. 2; the second is the region 200–280 Å, showing most of the structure observed, shown in Figs. 3 and 4; and finally, two discrete low-contrast structures at 146 and 168 Å which appear only in the summary table.

The splitting of the $2s^2\,2p^5\,{}^2P^\circ$ term of Ne II is about 0.1 eV or 2.5 Å. High members of series converging to the upper, $^2P_{1/2}{}^\circ$, limit lie therefore above the lower limit and may interfere with the continua $2s^2\,2p^5\,{}^2P_{3/2}{}^\circ\epsilon s$ and ϵd. These auto-ionized spectral features are completely analogous to those observed by Beutler[13] in argon, krypton, and xenon, and qualitatively interpreted by Fano.[14] In neon the limit is at considerably higher

[13] H. Beutler, Z. Phys. **93**, 177 (1935).
[14] U. Fano, Nuovo Cimento **12**, 156 (1935).

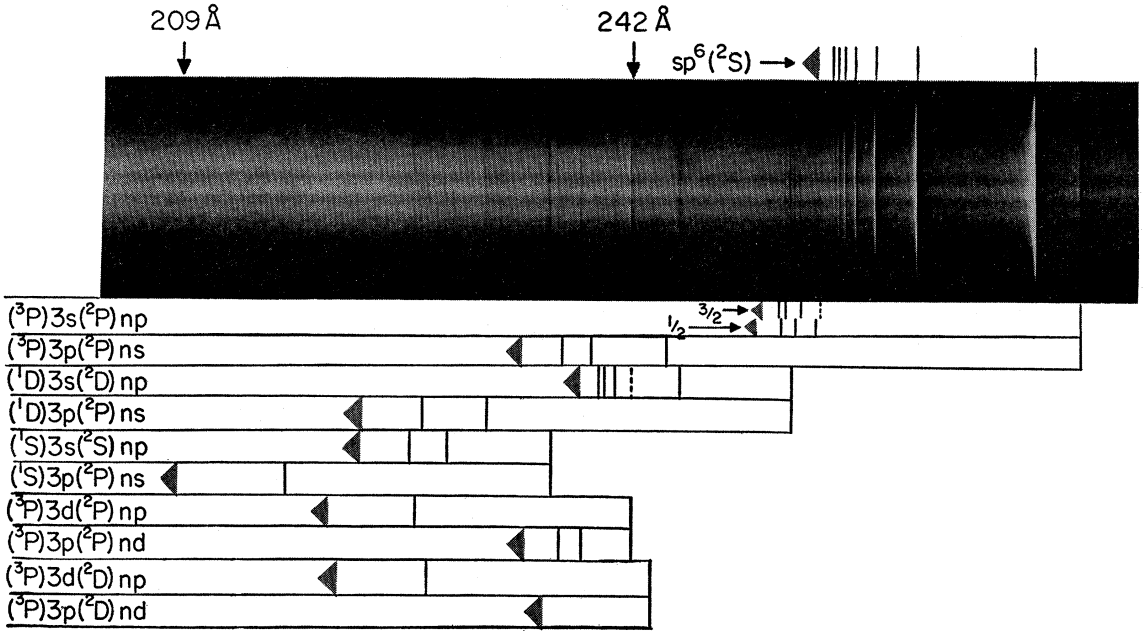

FIG. 3. The absorption spectrum of neon in the 200–280 Å region, showing (to the right) the strong asymmetric resonances due to the excitation of a subshell $2s$ electron. The remaining weaker structures are due to the simultaneous excitation of two $2p$ electrons. (The photograph is a positive print and therefore black denotes absorption.)

energy and the splitting is smaller; and these transitions have not previously been observed. A densitometer trace of the spectrum plate is shown in Fig. 2. This region was photographed using a path length of 110 cm and a pressure of approximately 0.1 Torr.

The absorption spectrum of Ne I in the 200–280 Å (~44–62 eV) spectral region contains many discrete features. This region was studied using pressures ranging from 0.02–0.20 Torr and a path length of 85–90 cm. The photograph in Fig. 3 was taken at a pressure of 0.2 Torr. Since this region is well above the 1st ionization potential for neon, the discrete structure appearing in Fig. 3 is superimposed on a continuous background absorption, owing to the transitions

$$2s^2\,2p^6\,{}^1S_0 \rightarrow 2s^2\,2p^5\,\epsilon s \text{ and } \epsilon d.$$

Transitions to five terms of these final configurations would be allowed in jj coupling and only two in strict LS coupling. Ne I is, generally, intermediate between these two cases. The photograph in Fig. 3 is a positive print; therefore, dark zones in the spectrum represent increased absorption. The discrete structure is observed as variations in the background absorption, i.e., resonances.

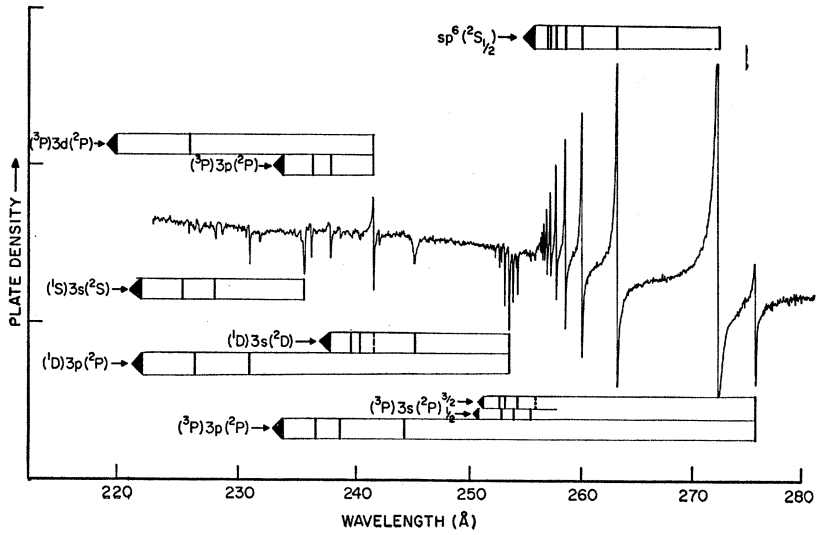

FIG. 4. A densitometer trace of the spectrum shown in Fig. 3, indicating more clearly the weaker resonance profiles. The series members are indicated and the limits identified.

TABLE I. Wavelength, wavenumber and effective quantum number (n^*) for the high members of the $2s^2\,2p^6\,{}^1S_0 \rightarrow 2s^2\,2p^5(^2P_{1/2,3/2})ns,nd$ series in Ne I.

Wavelength (Å)	Wave number (cm^{-1})	Designation	n^*
577.19(±0.01)[a]	173 253	$14s[1\frac{1}{2}]^\circ$	12.73
577.11	173 277	$13d[\frac{1}{2}]^\circ$&$[1\frac{1}{2}]^\circ$	12.96
576.88	173 346	$15s[1\frac{1}{2}]^\circ$ $9d'[1\frac{1}{2}]^\circ$	13.71 8.97
576.82	173 364	$14d[\frac{1}{2}]^\circ$&$[1\frac{1}{2}]^\circ$	13.92
576.58	173 436	$16s[1\frac{1}{2}]^\circ$ $15d[\frac{1}{2}]^\circ$&$[1\frac{1}{2}]^\circ$	14.90
576.40	173 491	$17s[1\frac{1}{2}]^\circ$ $16d[\frac{1}{2}]^\circ$&$[1\frac{1}{2}]^\circ$	15.81
576.21	173 548	$18s[1\frac{1}{2}]^\circ$ $17d[\frac{1}{2}]^\circ$&$[1\frac{1}{2}]^\circ$	16.95
575.00	173 913	$13s'[\frac{1}{2}]^\circ$	11.73
574.94	173 930	$^2P_{3/2}$ limit	
574.89	173 946	$12d'[1\frac{1}{2}]^\circ$	11.98
574.60	174 034	$14s'[\frac{1}{2}]^\circ$	12.74
574.53	174 055	$13d'[1\frac{1}{2}]^\circ$	12.94
574.24	174 143	$15s'[\frac{1}{2}]^\circ$ $14d'[1\frac{1}{2}]^\circ$	13.91
574.00	174 216	$16s'[\frac{1}{2}]^\circ$ $15d'[1\frac{1}{2}]^\circ$	14.90
573.80	174 277	$17s'[\frac{1}{2}]^\circ$ $16d'[1\frac{1}{2}]^\circ$	15.92
573.63	174 328	$18s'[\frac{1}{2}]^\circ$ $17d'[1\frac{1}{2}]^\circ$	16.95
572.38	174 710	$^2P_{1/2}$ limit	

[a] Error quoted represents the relative uncertainty in the measurements. They are put on an absolute basis by comparison with earlier work [Reference 15, and B. Peterson, Ark. Fys. 27, 317 (1965)].

The resonances which are caused by single-electron excitation states appear in the spectrum with high contrast. They form the strong Rydberg series of asymmetric features to the right in Fig. 3. By comparison, the remaining resonances, which are due to states involving the simultaneous excitation of two electrons, have lower contrast. Many very weak resonances can be seen on the photographic plates which, unfortunately, are not visible in the reproduction of Fig. 3. In an attempt to portray some of these weaker resonances, a densitometer trace of a portion of this photographic plate is shown in Fig. 4. Not all of the observed and listed resonances can be demonstrated by a densitometer trace—the weakest ones require examination of the photographic plates by eye. All of the resonances observed with certainty in this region (200–280Å) are listed in Table II.

The low-contrast resonances found at 146 and 168 Å required a neon pressure of 0.2 Torr, with a path length of 78 cm. Because of the continuum absorption, exposures of 4 h of synchrotron on-time were required to bring out this region of the spectrum.

IV. CLASSIFICATION OF SPECTRA

A. 570–580 Å Region

Five Rydberg series of absorption lines have been observed converging to the lowest term in Ne II, as seen in Fig. 2. Three of these converge to the lower $^2P_{3/2}{}^\circ$ limit (the series marked "nd" is actually double), the remaining series to the higher $^2P_{1/2}{}^\circ$ limit. These five series represent all of the possible transitions from the ground state to $J=1$ final states of the type

$$2s^2\,2p^6\,{}^1S_0 \rightarrow 2s^2\,2p^5(^2P)ns \quad \text{and} \quad 2s^2\,2p^5(^2P)nd.$$

LS-coupling does not hold for these states of neon. In jl notation,[15] the configurations associated with the series which converge to the lower limit are: $ns[\frac{1}{2}]^\circ$, $nd[\frac{1}{2}]^\circ$, $nd[1\frac{1}{2}]^\circ$, while those associated with the series converging to the upper limit are $ns'[\frac{1}{2}]^\circ$ and $nd'[1\frac{1}{2}]^\circ$.

For the latter two series, the members with n greater than 14 and 12, respectively, lie above the $^2P_{3/2}{}^\circ$ limit. Thus they can interact with the adjacent continua $2s^2\,2p^5(^2P_{3/2})\epsilon s$ and ϵd. There is insufficient resolution in Fig. 2 to establish the profiles of those lying below the limit. It is expected, however, that if higher resolution were available, the high-lying members would appear broadened by auto-ionization and that their profiles might be similar to the "Beutler-Fano" profiles observed in Ar, Kr, and Xe.

It is interesting to note that the series member $13s'[\frac{1}{2}]^\circ$ is similar to the higher members of its series although it lies below the $^2P_{3/2}{}^\circ$ limit, and that the inflection point of the sharp increase in absorption occurs at about 0.13 Å below the $^2P_{3/2}{}^\circ$ limit. There is, of course, no jump in cross section at an ionization limit, i.e., the average cross section over a small spectral region just below the limit is equal to the average cross section of a similar small region just above the limit.

The step in cross section actually occurs high in the series where the Doppler widths of the absorption lines become comparable with the spacing between adjacent series members; and the absorption becomes truly continuous in nature. Experimentally, this step is often exaggerated since absorption rather than cross section is observed. The average cross section remains essentially constant throughout the series; however, below the point of Doppler merging, the oscillator strength is packed into lines—thus the peak values of the cross section for the lines are higher than that in the continuum. Under most experimental conditions, the density of gas is high enough to "blacken" these lines at their centers. The experimentally observed absorption, however, may be considerably less due to insufficient resolution. This "underestimate" of the strength of the lines makes the absorption step more pronounced.

The series member $13s'[\frac{1}{2}]^\circ$, which lies below the $^2P_{3/2}{}^\circ$ limit, can nevertheless interact with the continua of Doppler-broadened lines high in the series converging to the $^2P_{3/2}{}^\circ$ limit.

In Table I a number of members of the five series occurring below the $^2P_{3/2}{}^\circ$ limit are listed. While these

[15] *Atomic Energy Levels*, edited by C. E. Moore, Natl. Bur. Stds. (U. S.) Circ. No. 467 (U. S. Government Publishing and Printing Office, Washington, D. C., 1949), Vol. I.

apparently have not been observed before, their locations are calculable by extrapolation from emission data on the lower members, to at least the accuracy of our measurements. The positions of the members of the two series $ns'[\frac{1}{2}]^\circ$ and $nd'[\frac{1}{2}]^\circ$ occurring above the lower absorption edge have been measured at the absorption maxima. For the first few of these, as seen in Fig. 2, the ns' and nd' series are just resolvable. These measurements of the absorption peaks above the limit are quite compatible with the quantum defects of the members of these series lying below the $^2P_{3/2}{}^\circ$ limits, i.e., there appears to be no perturbation as the series develops beyond the $^2P_{3/2}{}^\circ$ limit.

B. 255–280 Å Region—One-Electron Excitation

The prominent series of asymmetric resonances appearing in the right half of the spectrogram of Fig. 3 and the densitometer trace in Fig. 4 is due to the existence of excitation states for the subshell "s" electron in neon. Thus, the transitions can be described as

$$2s^2\,2p^6\,{}^1S_0 \rightarrow 2s\,2p^6({}^2S)np\,{}^1P_1{}^\circ.$$

While similar levels of $^3P_1{}^\circ$ character exist, only a single series can be distinguished. Unless the $^3P_1{}^\circ$ series is unresolvable from the $^1P_1{}^\circ$ series, the implication is that LS-coupling is dominant for this configuration of Ne I.

The profiles of this series of optically excited resonances will be discussed in Sec. V. Here it will be sufficient to mention that the series members have quantum defects quite similar to those of configurations involving p electrons in Ne I, and that the series converges in an unperturbed manner to the $2s\,2p^6\,{}^2S_{1/2}$ state of Ne II. The positions of the resonances in this series have been measured at the absorption maxima. They are included in the general table for all resonances seen in the 200–280 Å region (Table II). The energies of these excited states have recently been calculated theoretically[3,16] by a Hartree-Fock method yielding quite satisfactory agreement with the experimental values.

C. 200–280 Å Region—Two-Electron Excitation

Section IV B dealt with the only one-electron excitation configuration to which optical transitions from the ground state can be realized in this energy region. (The K-shell ionization occurs at ~14.3 Å). Thus, the additional discrete structure observed in the 200–280 Å region must be due to multiple electron excitation. Transitions to states of the type $2s^2\,2p^4\,nln'l'$ would be the lowest energy possibilities. But let us consider for a moment the next highest energy two-electron excitation states, namely $2s\,2p^5\,nln'l'$. The lowest energy possibility of this type would be $2s\,2p^5\,3s^2$. A rough estimate of the lowest possible energy for this configuration is about 565 000 cm^{-1}, corresponding to a wavelength of 180 Å. Excitations of this type are not, therefore, expected in the 200–280 Å region.

A further possibility which can also be ruled out is the excitation of more than two-electrons. The energy required to excite three of the outer p electrons in neon to the lowest energy configuration is again estimated to lie outside the 200–280 Å region. Furthermore, most of the observed two-electron excitation structures are weaker than the one electron structures by one or two orders of magnitude. Spectra due to three-electron excitation states, if weaker again by this amount, would probably be unobservable in these experiments.

We are left, then, with configurations of the type $2s^2\,2p^4\,nln'l'$ to explain the observed structure. More specifically, from consideration of two-electron excitation selection rules,[17] the following transitions are most probable:

$$2s^2\,2p^6 \rightarrow \begin{cases} 2s^2\,2p^4\,3s\;np \text{ (or } 3p\;ns), \\ 2s^2\,2p^4\,3p\;nd \text{ (or } 3d\;np), \\ 2s^2\,2p^4\,3s\;nf \text{ (or } 4f\;ns), \\ 2s^2\,2p^4\,3d\;nf \text{ (or } 4f\;nd). \end{cases}$$

All of these configurations have a common "grandparent." The four equivalent p electrons yield terms of the type $2s^2\,2p^4({}^3P,{}^1D,{}^1S)$. The final-state term system for each of the above configurations can then be determined by adding on the two remaining electrons. As an example, for the $2s^2\,2p^4\,3s\,np$ configuration, we can write, using L-S notation:

$$2s^2\,2p^4\begin{Bmatrix}{}^3P\\{}^1D\\{}^1S\end{Bmatrix}3s\begin{Bmatrix}{}^{2,4}P\\{}^2D\\{}^2S\end{Bmatrix}np\begin{Bmatrix}{}^{1,3}(S^\circ,P^\circ,D^\circ);{}^{3,5}(S^\circ,P^\circ,D^\circ)\\{}^{1,3}(P^\circ,D^\circ,F^\circ)\\{}^{1,3}P^\circ\end{Bmatrix}.$$

In this array, the final terms are formed from the parent and grandparent terms on the same horizontal line by the addition of the indicated electron. Since the ground state for all observed transitions must be $^1S_0$, we need consider only the final states having $J=1$. In the ordinary Ne I spectrum, as has been mentioned, the coupling of the excited electron to the core is intermediate between LS- and jj-coupling. The spectrum of Ne II on the other hand is adequately described in an LS-coupling scheme. If jj- or jl-coupling were appropriate for Ne I with two excited electrons, all $J=1$ final states would have to be considered, i.e., in the example of the configurations $2s^2\,2p^4\,3s\,np$, given above, there are 14 such $J=1$ levels. We have found the two-electron excitation spectrum of Ne I sufficiently simple that virtually all of the observed structure can be accounted for by assuming LS coupling, with one exception which will be discussed later.

Restricting ourselves now to pure LS coupling, only $^1P_1{}^\circ$ final-state levels are considered. Thus for the

[16] A. Weiss (private communication).

[17] S. Goudsmit and L. Gropper, Phys. Rev. 38, 225 (1931).

TABLE II. All observed resonances in the photoionization continuum of Ne I, in the region 80–570 Å.

Wavelength (Å)	Wave number (cm^{-1})	Identification	n^*	Type	Intensity
275.64(±0.05)[a]	362 790	$2p^4(^3P)3s(^2P)3p\ ^1P_1^\circ$	1.765	As[b]	25[c]
272.21(±0.05)	367 360	$2s^2\ p^6(^2S_{1/2})3p\ ^1P_1^\circ$	2.155	As	100
263.11	380 069	$2s^2\ p^6(^2S_{1/2})4p\ ^1P_1^\circ$	3.171	As	70
259.96	384 675	$2s^2\ p^6(^2S_{1/2})5p\ ^1P_1^\circ$	4.17	As	50
258.48	386 877	$2s^2\ p^6(^2S_{1/2})6p\ ^1P_1^\circ$	5.17	As	35
257.68	388 078	$2s^2\ p^6(^2S_{1/2})7p\ ^1P_1^\circ$	6.15	As	25
257.19	388 818	$2s^2\ p^6(^2S_{1/2})8p\ ^1P_1^\circ$	7.12	As	15
256.85	389 332	$2s^2\ p^6(^2S_{1/2})9p\ ^1P_1^\circ$	8.16	As	10
256.63	389 666	$2s^2\ p^6(^2S_{1/2})10p\ ^1P_1^\circ$	9.13	As	7
256.46	389 924	$2s^2\ p^6(^2S_{1/2})11p\ ^1P_1^\circ$	10.18	As	4
256.35	390 092	$2s^2\ p^6(^2S_{1/2})12p\ ^1P_1^\circ$	11.10	As	3
255.41	391 527	$2p^4(^3P)3s(^2P_{1/2})5p\ ^1P_1^\circ$	3.930	Ab	1
254.26	393 298	$2p^4(^3P)3s(^2P_{3/2})6p\ ^1P_1^\circ$ [d]	4.82	Ab	8
253.83	393 964	$2p^4(^3P)3s(^2P_{1/2})6p\ ^1P_1^\circ$	4.85	Ab	9
253.51	394 462	$2p^4(^1D)3s(^2D)3p\ ^1P_1^\circ$	2.060	Ab	16
253.12	395 070	$2p^4(^3P)3s(^2P_{3/2})7p\ ^1P_1^\circ$ [d]	6.10	Ab	12
252.81	395 554	$2p^4(^3P)3s(^2P_{1/2})7p\ ^1P_1^\circ$	5.97	Ab	3
252.65	395 804	$2p^4(^3P)3s(^2P_{3/2})8p\ ^1P_1^\circ$ [d]	7.03	Ab	4
252.33	396 306	$2p^4(^3P)3s(^2P_{3/2})9p\ ^1P_1^\circ$ [d]	8.00	Ab	1
252.28	396 385	$2p^4(^3P)3s(^2P_{1/2})8p\ ^1P_1^\circ$	6.98	Ab	1
252.12	396 637	$2p^4(^3P)3s(^2P_{3/2})10p\ ^1P_1^\circ$ [d]	8.90	Ab	1
251.95	396 904	$2p^4(^3P)3s(^2P_{1/2})9p\ ^1P_1^\circ$	7.96	Ab	1
245.20(±0.1)	407 830	$2p^4(^1D)3s(^2D)4p\ ^1P_1^\circ$	2.963	Ab	5
244.31	409 316	$2p^4(^3P)3p(^2P)4s\ ^1P_1^\circ$	2.417	As	1
243.10	411 353	$2p^4(^3P)3d(^2D)3p\ ^1P_1^\circ$	1.600	As	2
242.11	413 035	$2p^4(^1D)3s(^2D)4f\ ^1P_1^\circ$	3.879	As	3
241.8(±0.1)	413 560	$2p^4(^1D)3s(^2D)5p\ ^1P_1^\circ$	4.03	Ab	1
241.64	413 839	$2p^4(^3P)3d(^2P)3p\ ^1P_1^\circ$	1.628	As	15
240.45	415 887	$2p^4(^1D)3s(^2D)6p\ ^1P_1^\circ$	4.97	Ab	2
239.65	417 275	$2p^4(^1D)3s(^2D)7p\ ^1P_1^\circ$	5.99	Ab	1
239.16	418 130	$2p^4(^1D)3s(^2D)8p\ ^1P_1^\circ$	7.06	Ab	1
238.90(±0.1)	418 590	$2p^4(^1D)3s(^2D)9p\ ^1P_1^\circ$	7.93	Ab	1
238.76	418 831	$2p^4(^3P)3p(^2P)5s\ ^1P_1^\circ$	3.441	As	2
237.92	420 309	$2p^4(^3P)3p(^2P)4d\ ^1P_1^\circ$	3.753	As	6
236.67	422 529	$2p^4(^3P)3p(^2P)6s\ ^1P_1^\circ$	4.44	As	1
236.26	423 263	$2p^4(^3P)3p(^2P)5d\ ^1P_1^\circ$	4.76	As	4
235.65[e]	424 358	$2p^4(^1S)3s(^2S)3p\ ^1P_1^\circ$	2.045	Ab	10
235.45(±0.1)	424 720	$2p^4(^3P)3p(^2P)6d\ ^1P_1^\circ$	5.70	Ab	1
235.1(±0.1)[f]	425 350	$2p^4(^3P)3p(^2P)8s\ ^1P_1^\circ$	6.32	Br	1
234.7(±0.1)	426 080	$2p^4(^3P)3p(^2P)9s\ ^1P_1^\circ$	7.37	Br	1
230.98	432 938	$2p^4(^1D)3p(^2P)4s\ ^1P_1^\circ$	2.521	As	5
228.68(±0.05)	437 290	$2p^4(^1D)3d(^2D)3p\ ^1P_1^\circ$	1.600	Ab	2
228.10(±0.05)	438 400	$2p^4(^1S)3s(^2S)4p\ ^1P_1^\circ$	2.998	Ab	2
226.76(±0.05)	440 990	$2p^4(^3P)3d(^2D)4p\ ^1P_1^\circ$	2.882	Ab	2
226.37(±0.05)	441 750	$2p^4(^1D)3p(^2P)5s\ ^1P_1^\circ$	3.596	Ab	2
225.85(±0.05)	442 770	$2p^4(^3P)3d(^2P)4p\ ^1P_1^\circ$	2.964	As	2
225.41(±0.05)	443 640	$2p^4(^1S)3s(^2S)5p\ ^1P_1^\circ$	3.967	Ab	2
224.7(±0.1)	445 040	$2p^4(^1D)3p(^2P)6s\ ^1P_1^\circ$	4.61	Br	1
223.9(±0.1)	446 630	$2p^4(^1D)3p(^2P)7s\ ^1P_1^\circ$	5.60	Br	1
223.4(±0.1)	447 630	$2p^4(^1D)3p(^2P)8s\ ^1P_1^\circ$	6.52	Br	1
219.2(±0.1)	456 200	?	···	Br	1
218.5(±0.1)	457 670	?	···	Br	1
217.9(±0.1)	458 930	?	···	Br	1
216.50(±0.1)	461 890	$2p^4(^1S)3p(^2P)4s\ ^1P_1^\circ$	2.508	Br	2
215.35(±0.1)	464 360	$2p^4(^1S)3d(^2D)3p\ ^1P_1^\circ$	1.710	Ab	2
213.6(±0.1)	468 160	?	···	Br	1
211.80(±0.1)	472 140	?	···	Ab	2
211.48(±0.1)	472 900	?	···	Ab	2
210.2(±0.1)	475 740	?	···	Br	1
167.69(±0.1)	596 340	$2s2p^5(^3P)\ 3p^2\ ^1P_1^\circ$	?	As	2
145.98(±0.1)	685 030	$2s2p^5(^1P)\ 3p^2\ ^1P_1^\circ$	?	As	2

[a] Errors are estimated to be ±0.03 Å unless stated.
[b] As—asymmetric, Ab—absorption-type resonance, Br—broad, weak absorption-type resonance.
[c] The intensity figures quoted have only a rough significance.
[d] These levels cannot be pure $^1P_1^\circ$ in character.
[e] Overlaps line due to $2p^4(^3P)3p(^2P)7s\ ^1P_1^\circ$.
[f] Possible double line.

$2s^2\,2p^4\,3s\,np$ configuration, we can rewrite the above array as follows:

$$2s^2\,2p^4\begin{bmatrix}^3P\\ ^1D\\ ^1S\end{bmatrix}3s\begin{bmatrix}^2P\\ ^2D\\ ^2S\end{bmatrix}np\,^1P_1^\circ$$

and for the companion configuration $2s^2\,2p^4\,3p\,ns$

$$2s^2\,2p^4\begin{bmatrix}^3P\\ ^1D\\ ^1S\end{bmatrix}3p\begin{bmatrix}^2P\\ ^2P\\ ^2P\end{bmatrix}ns\,^1P_1^\circ,$$

that is, one $^1P_1^\circ$ Rydberg series of two-electron transitions would exist for each of the indicated parent terms. These six Rydberg series, three with a running s electron and three with a running p electron, would converge to the parent terms indicated (known states of Ne II). The six series would exist in three pairs, each having a common $3s\,3p$ member.

Turning now to final states of the $3p\,nd$ and $3d\,np$ configurations, and analyzing similarly for only the $^1P_1^\circ$ terms, we can form the following arrays:

$$2s^2\,2p^4\begin{bmatrix}^3P\\ ^1D\\ ^1S\end{bmatrix}3p\begin{bmatrix}^2P,^2D\\ ^2P,^2D,^2F\\ ^2P\end{bmatrix}nd\,^1P_1^\circ$$

and

$$2s^2\,2p^4\begin{bmatrix}^3P\\ ^1D\\ ^1S\end{bmatrix}3d\begin{bmatrix}^2P,^2D\\ ^2S,^2P,^2D\\ ^2D\end{bmatrix}np\,^1P_1^\circ.$$

Here we can expect 12 Rydberg series of $^1P_1^\circ$ levels, converging to the parent terms indicated. These would have only six $3p\,3d\,^1P_1^\circ$ levels, each common to two series.

In the case of the $3s\,nf$ and $4f\,ns$ configurations, the $^1P_1^\circ$ levels are restricted to the following:

$$2s^2\,2p^4(^1D)3s(^2D)nf\,^1P_1^\circ$$

and

$$2s^2\,2p^4(^1D)4f(^2P)ns\,^1P_1^\circ.$$

The resulting two Rydberg series, converging to the parent terms indicated, would have a common $3s\,4f$ member.

The final configurations to be considered, namely, $3d\,nf$ and $4f\,nd$, when analyzed for $^1P_1^\circ$ levels give the following arrays:

$$2s^2\,2p^4\begin{bmatrix}^3P\\ ^1D\\ ^1S\end{bmatrix}3d\begin{bmatrix}^2D,^2F\\ ^2D,^2F,^2G\\ ^2D\end{bmatrix}nf\,^1P_1^\circ$$

$$2s^2\,2p^4\begin{bmatrix}^3P\\ ^1D\\ ^1S\end{bmatrix}4f\begin{bmatrix}^2D,^2F\\ ^2P,^2D,^2F\\ ^2F\end{bmatrix}nd\,^1P_1^\circ.$$

Therefore, 12 series might be expected in six pairs having common first members, $3d\,4f$.

From a consideration of the binding energies of s, p, d and f electrons in Ne I and Ne II, and making a rough allowance for screening effects, it is possible to estimate the energy associated with the above configurations. However, these estimates are not sufficiently accurate to be of more than a general guideline in the analysis. Rather, we have attempted to organize the observed resonances into a scheme which is internally consistent with the above LS-coupling analysis of the most probable two-electron transitions. Consideration is also given to the profile, width and strength of the resonances which are grouped into a series. Unless there is an additional interaction effect, the members of a series tend to have similar profiles, and of course decreasing width and strength with increasing n.

Nearly all of the observed two-electron resonances have been assigned a classification according to the above scheme. These results are shown, in part, in Figs. 3 and 4, and are listed in Table II. The wavelength of these resonances, as listed, has been measured to the center of the absorption maximum for both the enhanced-absorption features and the asymmetric resonances. The intensity scale is a very rough evaluation—higher numbers mean greater contrast of the resonance with respect to the background absorption. Our identification of each resonance is indicated, as well as the effective quantum number consistent with the listed identification.

$2p^4\,3s\,np;\ 2p^4\,3p\,ns$

The most reliable identifications are the six series which exist for these configurations. Since Table II is primarily a "finding" list, the effective quantum numbers of the first four members of these six series are regrouped in Table III.

The lowest-lying series is associated with the lowest energy term of the grandparent configurations, $2p^4(^3P)$. The effective quantum numbers of the $3s\,np$ and $3p\,ns$ series associated with this grandparent term are also somewhat lower than those associated with the ^1D and ^1S grandparent terms. The $2p^4(^3P)3s\,3p\,^1P_1^\circ$ level, as seen from Fig. 2, lies even lower than the lowest $2s\,2p^6\,np\,^1P_1^\circ$ level, and is responsible for the strongest resonance seen in the two-electron excitation spectrum. Note that, from the standpoint of effective quantum numbers, the $2p^4(^3P)3s\,3p\,^1P_1^\circ$ level fits into a Rydberg

TABLE III. Observed effective quantum numbers of the $3s\,np$ and $3p\,ns$ series in Ne I for the three "grandparent" configurations $2p^4(^3P,^1D,^1S)$.

	$2p^4(^3P)3s(^2P)np$	$2p^4(^1D)3s(^2D)np$	$2p^4(^1S)3s(^2S)np$
$n^*(3p)$	1.765	2.060	2.045
$n^*(4p)$	···	2.963	2.998
$n^*(5p)$	3.930	4.03	3.967
$n^*(6p)$	4.85	4.97	···
	$2p^4(^3P)3p(^2P)ns$	$2p^4(^1D)3p(^2P)ns$	$2p^4(^1S)3p(^2P)ns$
$n^*(3s)$	1.296	1.403	1.413
$n^*(4s)$	2.417	2.521	2.508
$n^*(5s)$	3.441	3.596	···
$n^*(6s)$	4.44	4.61	···

scheme for the $3p\,ns$ series much better than for the $3s\,np$ series. While a number of high-lying members of the $2p^4(^3P)3s\,np$ series have been observed, it is interesting that the second, or $3s\,4p$, member of this series is missing. The reason for this missing member is not clear, at present; however we will comment further on this phenomenon in the final section dealing with configuration-interaction effects.

The resonances due to $3s\,3p$ levels constructed from the ^1D and ^1S grandparent terms are less prominent and have different profiles from those constructed from the ^3P grandparent. Since the levels involving the ^1D and ^1S grandparent lie higher in energy, there are additional continua with which they can interact.

From Fig. 2 and Table II, two $3s\,np$ Rydberg series can be seen converging onto the $2p^4(^3P)3s(^2P)$ term of the ion. A second series would not be allowed in strict LS-coupling, and appears to be the only evidence of a breakdown of this coupling scheme which we have seen. However, only one $2p^4(^3P)3s\,3p$ level has been seen.

$2p^4\,3p\,nd$; $2p^4\,3d\,np$

The assignments of terms to the 12 allowed series of the $3p\,nd$ and $3d\,np$ configurations are somewhat less reliable than for the $3s\,np$ and $3p\,ns$ configurations, mainly on account of their weak contrast. Of the six $3p\,3d\,^1P_1^\circ$ levels to be considered in strict LS coupling, we have assigned four. Transitions to the higher-energy levels would occur in a region of the spectrum where the contrast of the discrete structure with the background is very low. Apparently, these discrete levels interact with only a minor fraction of the continua available for dipole transitions from the ground state, resulting in resonances of weak contrast. The strongest of the $p\,d$ series, by far, is $2p^4(^3P)3p(^2P)nd\,^1P_1^\circ$ where several members are assigned. This series appears so much stronger than any of the other $p\,d$ series found that one questions somewhat the assignment. The resonances involved could conceivably be the higher members of the series $2p^4(^3P)3p(^2P)ns\,^1P_1^\circ$. However, a consideration of the quantum defects for these resonances, and of others available for this $3p\,nd$ series, makes our given assignment more plausible.

$2p^4\,3s\,nf$

It was pointed out earlier that in strict LS coupling a transition to only a single $3s\,4f$ level was expected, namely, $2p^4(^1D)3s\,4f\,^1P_1^\circ$. The appropriate state of the ion, namely, $2p^4(^1D)3s(^2D)$, is known, and since the f electron would be quite hydrogenic, a resonance due to this state should have an effective quantum number very close to 4. There is available in the spectrum an asymmetric resonance which has an n^* of 3.88 with respect to this limit. The defect, 0.12, is a little large for an f electron. However, it may be that the energy of this resonance is somewhat depressed by the proximity of the strong $2p^4(^3P)3p(^2P)3d\,^1P_1^\circ$ resonance. Further discussion of this point will be deferred to a later section on configuration interaction. No higher series members have been found, which may indicate that the $3s\,4f$ resonance is enhanced by interaction with its neighbor.

$2p^4\,3d\,nf$

None of the possible $3d\,4f\,^1P_1^\circ$ levels has been positively identified. Again their locations should be predictable by hydrogenic positioning the $3d\,4f\,^1P_1^\circ$ level below the known states of the ion corresponding to the $2p^4\,3d$ configuration. In most cases there is no resonance available in the vicinity. This may be expected since double electron transitions involving $\Delta l_1=1$, $\Delta l_2=2$ are less probable than those involving $\Delta l_1=1$, $\Delta l_2=0$.

D. 140–170 Å Region

We have observed two asymmetric resonances, having negative q, at 146 and 168 Å. These are listed at the end of Table II. The energy required to excite states in this region is obviously greater than that required to remove two $2p$ electrons in neon. Thus these resonances cannot be identified with configurations of the type $2s^2\,2p^4\,nl\,n'l'$. Since these also cannot involve a one-electron excitation, they must be due to a two-electron excitation of the type

$$2s^2\,2p^6 \rightarrow 2s\,2p^5\,nl\,n'\,l'.$$

Of the various possibilities, we would expect the most probable to be excitations to

$$2s\,2p^5\,ns\,n's \quad \text{or} \quad 2s\,2p^5\,np\,n'p.$$

The two observed resonances (of approximately equivalent strength) are too widely separated to belong to the same Rydberg series; hence, we need consider only first series members, i.e., $n=n'$.

The term analysis of these configurations is then

$$2s\,2p^5\begin{pmatrix}^3P\\ ^1P\end{pmatrix}3s^2\begin{pmatrix}^3P^\circ\\ ^1P^\circ\end{pmatrix}$$

and

$$2s\,2p^5\begin{pmatrix}^3P\\ ^1P\end{pmatrix}3p^2\begin{pmatrix}^{1,3,5}(S^\circ,P^\circ,D^\circ);\,^3(S^\circ,P^\circ,D^\circ);\,^3P^\circ\\ ^3(S^\circ,P^\circ,D^\circ);\,^1(P^\circ,D^\circ,F^\circ);\,^1P^\circ\end{pmatrix}.$$

The energy of these configurations can be estimated from the known energy of the $2s\,2p^5$ configuration, the binding energy of $3l$ electrons, and an empirically based estimate of the mutual screening of the two excited electrons. These estimates are in poor agreement with the choice of the configuration $2s\,2p^5\,3s^2$. Here, the estimated energy is too low even before the depression due to screening is evaluated. Furthermore, the two observed resonances are of roughly equal strength, which is incompatible with the fact that the configuration $2s\,2p^5\,3s^2$ has only one $^1P_1^\circ$ level, and LS coupling appears to be a reasonable assumption for the two-electron excitation of neon. In contrast, the estimates

are in good agreement with the choice of the configuration $2s\,2p^5\,3p^2$, and favor the assignment of both resonances to $2s\,2p^5\,3p^2$ rather than one to $2s\,2p^5\,3p^2$ and the other to $2s\,2p^5\,3s^2$. From the term analysis above, we realize that two $^1P_1^\circ$ levels can be associated with the ^1P term of the $2s\,2p^5$ grandparent configuration, and one $^1P_1^\circ$ level with the ^3P term of the grandparent. The known $^3P_1$–$^1P_1$ separation of the $2s\,2p^5$ configuration of Ne III is 84 600 cm^{-1}. The separation of the observed resonances is 88 600 cm^{-1}, which suggests that one of the resonances is associated with the level $2s\,2p^5(^3P)3p^2\,^1P_1^\circ$ where the two $3p$ electrons couple to form a ^3P, and the other resonance is associated with the level $2s\,2p^5(^1P)3p^2\,^1P_1^\circ$ where the two $3p$ electrons couple to form either a ^1D or ^1S. Hand-waving arguments suggest the $3p^2\,^1S$, but we prefer to leave this point to the theoretician. With either choice, we are left with a missing $^1P_1^\circ$ level of the configuration $2s\,2p^5(^3P)3p^2$.

V. RESONANCE PROFILES

A. Theory

The expected absorption profile of resonances in the photoionization continua of atoms due to the interference of high lying states with the continua has been formulated by Fano and Cooper.[2] Accordingly, this interference results in an absorption cross section of the form

$$\sigma=\sigma_1\frac{(q+\epsilon)^2}{1+\epsilon^2}+\sigma_2. \qquad (1)$$

Here, σ_1, is the background cross section associated with the fraction of the available continua with which the discrete state interacts, while σ_2 is the remaining background cross section, associated with the fraction of the continua which does not enter into the interaction. Thus, far from the resonance, $\sigma=\sigma_1+\sigma_2$. The ratio $\sigma_1/(\sigma_1+\sigma_2)=\rho^2$ defines ρ, the correlation index, which may be thought of as measuring the projection of the final state vector (after auto-ionization) upon the state vector representing the combined continuum in absence of the discrete state.

In (1), ϵ is an energy parameter, measuring displacement from some energy within the resonance, in units of the half-width of the discrete state, $\Gamma/2$. The parameter q, referred to as the profile index, is determined by the autoionization and transition matrix elements and can often be assumed constant over a given resonance. The quantities q and ρ^2 determine the resonance profile "type," as illustrated in Fig. 5. Note that for constant ρ^2, increasing q causes the absorption enhanced zone to grow strong relative to the reduced absorption zone. In this case if ρ^2 is also large, the resonance will appear quite asymmetric, but if ρ^2 is small the resonance will appear as an absorption line superimposed on a continuous background. A change in the sign of q reverses the asymmetry of the resonance.

B. Experimental Profiles

The absorption profiles of four of the most prominent resonances were obtained using the grazing-incidence monochromator. These were the one-electron excitation resonances $2s\,2p^6\,np\,^1P_1^\circ$ with the $n=3$, 4, and 5, and the lowest-lying (the most prominent) two-electron excitation resonance, $2s^2\,2p^4(^3P)3s\,3p\,^1P_1^\circ$. The mode of operation of the monochromator was discussed in Sec. II above. Typical scans of the transmission of neon at these resonances are illustrated in Fig. 6. The signal-to-noise ratio is limited by the rather low counting rates associated with the relatively high resolution utilized (0.065 Å). Our results, however, have considerably improved statistics over that observed in Fig. 6, since each of these resonances was scanned many times, using a variety of pressures. For each of these scans, a theoretical curve was fitted in the following way: First, using an educated guess for values of q, Γ, and ρ^2, a theoretical cross section was calculated. From this cross section, a theoretical transmission was calculated, and smeared by a Gaussian slit function of 0.065 Å half-maximum width. Finally the result was compared with the experimental data. This comparison allowed a better choice of values of q, Γ, and ρ^2, and the whole calculation was recycled until no further improvement was possible. From these calculations it was also possible to estimate

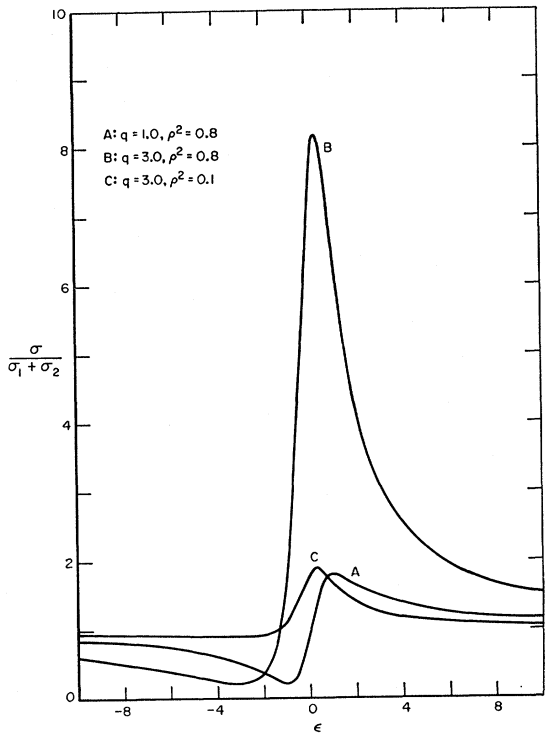

FIG. 5. A plot of three theoretical resonance profiles, showing the effect on the line shape of (i) increasing profile index (q) and (ii) reducing the autocorrelation coefficient (ρ^2). The cross section is normalized to 1 in the wings and plotted as a function of a reduced energy variable ϵ.

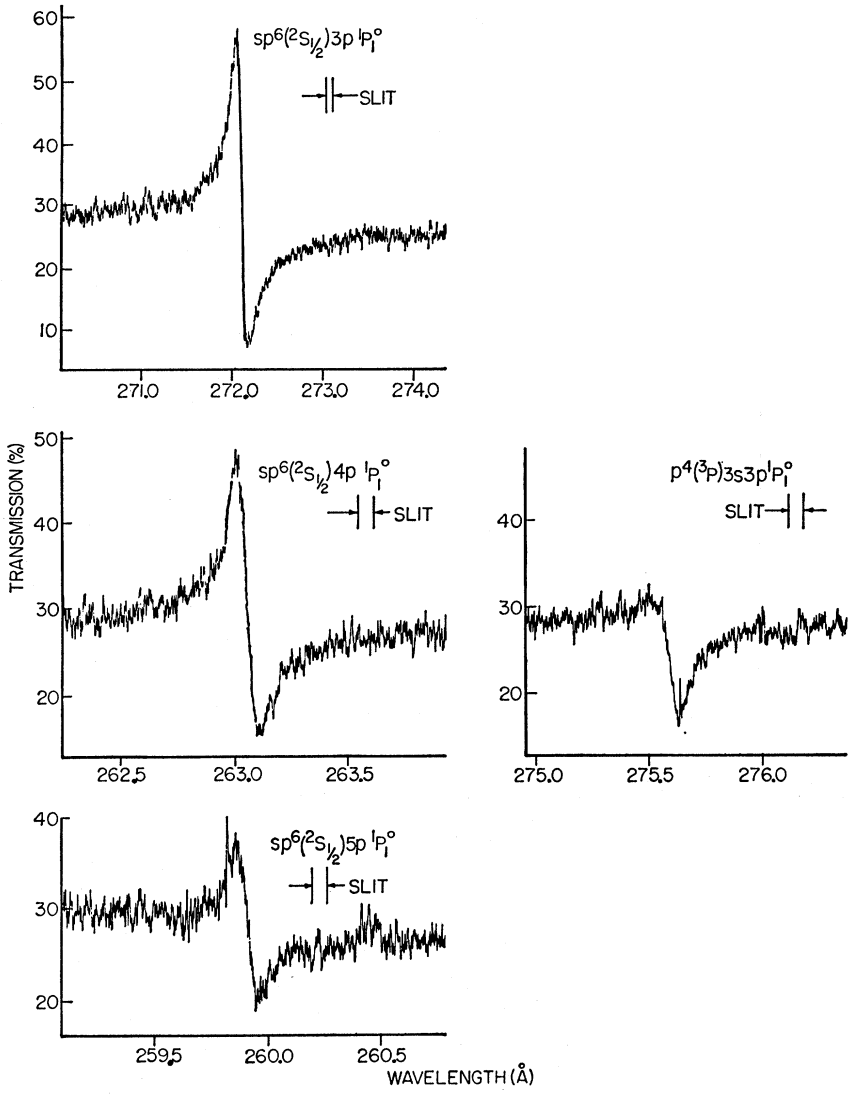

FIG. 6. Recorder tracings of the four strong resonances near 270 Å in the photo-ionization continuum of Ne I. For each of these scans, the pressure ≈0.05 Torr, path length ≈90 cm, counting rate in the wings ≈250 counts/sec, electronics time constant =2 sec, and the scanning time for each resonance ≈15 min. Note that the wavelength scale on the top trace is 2½ times more compact. Note also, the difference in appearance of the $2p^6\,4p$ and $2p^4\,3s\,3p$ resonances (middle traces). The oscillator strengths of these two resonances are comparable, but the value of ρ^2 for the two-electron excitation resonance is considerably smaller (see Table IV).

the uncertainty in the choice of the shape parameters. The values of q, Γ, and ρ^2 with the uncertainty determined from these curve fittings are given in Table IV.

One-Electron Excitation Resonances

The three resonances measured involving the levels $2s\,2p^6\,np\,{}^1P_1^\circ$ can be simply related. As predicted[2] for Rydberg series members which occur in an energy region where the matrix elements involved have a negligible variation, the values of q and ρ^2 for all three resonances are the same to within the error of measurement. Thus, these resonances can be represented by a single profile with $q=1.6$ and $\rho^2=0.70$, as shown in Fig. 7, curve A. The experimental values of q, Γ, and ρ^2

TABLE IV. Experimentally observed parameters for the four strong resonances near 270 Å in the photo-ionization continuum of Ne I.

	$2s\,2p^6\,3p\,{}^1P_1^\circ$	$2s\,2p^6\,4p\,{}^1P_1^\circ$	$2s\,2p^6\,5p\,{}^1P_1^\circ$	$2s^2\,2p^4\,3s\,3p\,{}^1P_1^\circ$
E (eV)	45.546(±0.008)[a]	47.121(±0.005)	47.692(±0.005)	44.979(±0.008)
q	−1.6(±0.2)	−1.6(±0.3)	−1.6(±0.5)	−2.0(±0.3)
Γ (eV)	0.013(±0.002)	0.0045(±0.0015)	0.002(±0.001)	0.010(±0.003)
ρ^2	0.70(±0.07)	0.70(±0.07)	0.70(±0.14)	0.17(±0.05)
σ_B (cm^{-1})[b]	230(±15)	215(±15)	220(±15)	225(±15)
$10^4 f$	17.4(±2.0)	5.6(±2.0)	2.6(±2.0)	6.1(±1.5)

[a] Errors quoted are our estimated uncertainties.
[b] σ_B is the background continuum cross section extrapolated to the center of the resonance, i.e., $\sigma=\sigma_1+\sigma_2$.

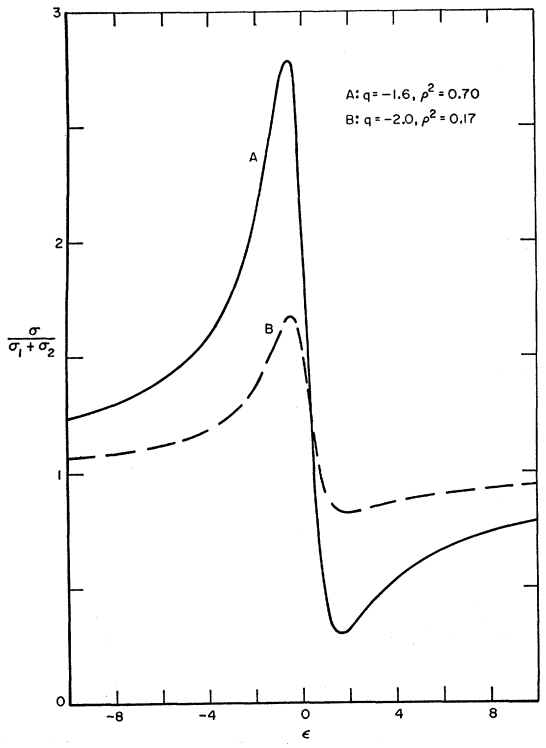

FIG. 7. Theoretical resonance profiles which best fit the experimentally observed shapes due to transitions from $2s^2\,2p^6\,{}^1S_0$ to: (A) the single electron excitation states $2s\,2p^6\,np\,{}^1P_1^\circ$, where $n=3$, 4 and 5, and (B) the two-electron excitation state $2p^4({}^3P)3s\,3p\,{}^1P_1^\circ$.

for the $n=3$ member of this series compare quite favorably with those calculated by Fano and Cooper[2] for this resonance. Reference 2 also suggests a semi-empirical formula to relate the widths of resonances in an unperturbed Rydberg series, namely: $\Gamma_n=Cn^*/(n^{*2}-1)^2$ where C is a constant for the series. The experimental widths, given in Table IV, are more favorably related by the formula

$$\Gamma_n=\text{const}/n^{*3},$$

to which they conform within the experimental error.

The excess oscillator strength for each resonance, given by $f=k(\sigma_1+\sigma_2)\frac{1}{2}\pi\Gamma\rho^2(q^2-1)$ where $k=3.39\times10^{-4}$ eV^{-1} cm, is also tabulated in Table IV. With the assumption that $\Gamma\sim n^*/(n^{*2}-1)^2$, which we are not able to confirm, the increase in continuum oscillator strength due to the opening of the $2s^2\,2p^6\,{}^1S_0\rightarrow 2s\,2p^5\,\epsilon p\,{}^1P_1^\circ$ channel for photo-ionization can be calculated from these excess oscillator strengths.[2] The calculation implies, essentially, that the average oscillator strength per unit energy in the continuum of this channel is the same as exists in the discrete spectrum. The result of this calculation is that the total continuum cross section is increased by approximately 0.5% due to the opening of this channel. This small increase reflects the fact that the resonances due to transitions to the $2s\,2p^6\,np$ configuration are small in oscillator strength, in spite of their prominence due to interference.

Two-Electron Excitation Resonance

The resonance caused by excitation to the $2s^2\,2p^4({}^3P)3s\,3p\,{}^1P_1^\circ$ state has values of q and ρ^2 which are similar to those of the most prominent one-electron excitation resonance, $2s\,2p^6\,3p\,{}^1P_1^\circ$. However, the value of ρ^2 is much lower for the two-electron excitation resonance, indicating that this state interacts with a smaller fraction of the continua available for dipole transitions from the ground state. The cross section versus ϵ for this resonance is given in Fig. 7, curve B, where the effect of the smaller correlation index and a slightly higher value of q can be noted by comparing it to curve A in the same figure.

The excess oscillator strength of this resonance, roughly comparable with the $n=4$ member of the one-electron series, is given in Table IV. The increase in continuum oscillator strength due to the opening of this two-electron excitation channel could be calculated in a similar manner as was done for the one-electron excitation channel above; however, because of complicating configuration-interaction effects in the $2p^4({}^3P)3s\,np$ series, the assumptions required for the calculation appear invalid.

VI. ADDITIONAL CONSIDERATIONS OF CONFIGURATION INTERACTION

In this section we would like to discuss a number of intensity anomalies, some of which have been mentioned briefly, which can be qualitatively explained by interactions which have not already been considered. As experimentalists, we do this empirically to establish order in the data and hope for theoretical arguments to strengthen or alter these suggestions.

Primarily, there is a strong indication that the two-electron configurations built on the $2s^2\,2p^4({}^3P)$ and $2s^2\,2p^4({}^1D)$ grandparents interact rather strongly. First, consider the series $2s^2\,2p^4({}^3P)3s({}^2P)np\,{}^1P_1^\circ$. The first member of this series, $3s\,3p\,{}^1P_1^\circ$ [which is also the first member of $2s^2\,2p^4({}^3P)3p({}^2P)ns$], is the strongest of the two-electron excitation resonances. The $n=4$ member is missing altogether, a point which we will return to later. The $n=5$ member appears weakly, $n=6$ and 7 are stronger, and the series fades with $n=8$, 9, and 10. Further, for $n=6$ through 9 two series can be identified, in the only positively established violation of strict LS coupling in the two-electron excitation spectrum of neon. At the intensity maximum of these series, between $n=6$ and $n=7$, appears the first member of the series $2p^4({}^1D)3s({}^2D)np$. The fact that this $2p^4({}^1D)3s\,np$ series is interacting strongly with the $2p^4({}^3P)3s\,np$ series is well established from the following experimental evidence:

1. The effective quantum numbers of the $n=5$, 6 members of the $2p^4(^3P)3s(^2P)np$ series are displaced to lower values, and the $n=7$, 8, 9 members are displaced to higher values, than expected for unperturbed Rydberg series.

2. The second member of the $2p^4(^1D)3s\,np$ series, namely, $2p^4(^1D)3s(^2D)4p\ ^1P_1^\circ$, is substantially broader than the first member, in opposition to the expected relative widths of successive auto-ionized levels in a series. The higher members of the $2p^4(^1D)3s\,np\ ^1P_1^\circ$ series are also broader than would be expected from the width of the first member. We suggest that the $n=4$ and higher members of this series suffer an additional broadening due to the interaction of these discrete resonances with the new continuum $2p^4(^3P)3s\,\epsilon p$, which is not available to the $2p^4(^1D)3s\ 3p\ ^1P_1^\circ$ level.[18]

3. The intensity, if not the very observance, of the $n=5$ through 10 members of the $2p^4(^3P)3s\,np$ series is difficult to account for except by an intensity-sharing interaction with the $2p^4(^1D)3s\ 3p\ ^1P_1^\circ$ resonance. The strong $n=3$ member should perhaps be thought of as belonging to the $2p^4(^3P)3p\,ns\ ^1P_1^\circ$ series with which it has a more compatible effective quantum number. This would also explain why the $n=4$ member of the $2p^4(^3P)3s\,np$ series has not been observed, although its expected position is sufficiently separated from the $n=5$ member of the $2s\,2p^6\,np\ ^1P_1^\circ$ series to be resolved.[19] Also, this $n=5$ member is neither perturbed from its expected Rydberg location, nor does it appear to suffer any intensity anomaly.

Another intensity discrepancy which suggests the strong interaction of the two-electron configurations involving the $2p^4(^1D)$ and $2p^4(^3P)$ grandparents exists for the resonance assigned to the $2p^4(^1D)3s\ 4f\ ^1P_1^\circ$ level. No other resonances have been observed which could be assigned to configurations of the type $2p^4\,nl\,n'f$. While these might be expected to be weak because of the small overlap of the f electron wave function with that of the $2s^2\,2p^6$ ground state, the appearance of a moderately strong resonance due to the $2p^4(^1D)3s\ 4f\ ^1P_1^\circ$ level, in the absence of the others, begs an explanation. It may be that this level interacts with the neighboring $2p^4(^3P)3p\ 3d\ ^1P_1^\circ$ level borrowing sufficient intensity to make it observable. If this interaction exists, it would be expected that the $2p^4(^1D)3s\ 4f\ ^1P_1^\circ$ level would be slightly displaced to lower energy. We note that the effective quantum number of this resonance (in Table II) is 3.88, which is indeed low for a typical hydrogenic f electron.

VII. FINAL REMARKS

Table I includes all of the resonances which we have observed between the $2s\,2p^5\ ^2P_{3/2}^\circ$ and $^2P_{1/2}^\circ$ ionization limits of Ne I. The "finding" list (Table II) contains all of the resonances we have observed from the $2s^2\,2p^5\ ^2P_{1/2}$ limit at 573 Å out to approximately 80 Å. A classification has been suggested for nearly all of the observed resonances. Unfortunately, the weakest can be observed only by examination of the original plates or high-quality photographs. We will try to make the latter available to those who wish to extend or revise the analysis.

The further understanding of this discrete spectrum requires accurate theoretical calculations of energies, transition probabilities and configuration-interaction effects.

Experimentally improved spectra would be attainable if the background continuum light source were stronger, thus making it possible to use higher pressures to bring up the resonances of lower contrast. Higher resolution would be of little aid in bringing out the weak resonances due to their large widths, but would be helpful in studying the profiles of the narrower resonances.

---

[18] The additional broadening of the $2p^4(^1D)3s\ 4p\ ^1P_1^0$ level can be used to estimate the interaction of the $2p^4(^1D)3s\,np$ with the $2p^4(^3P)3s\epsilon p$ configuration. A semiquantitative calculation by H. Mendlowitz has verified that the strength of the interaction, predicted in this way, is appropriate to explain the observed repulsion of the high members of the $2p^4(^3P)3s\,np$ series by the $(^1D)3s\ 3p\ ^1P_1^\circ$ resonance.

[19] We are indebted to U. Fano for the suggestion of this intensity sharing, and the attendant plausible explanation of the missing $n=4$ member of the $2p^4(^3P)3s\,np$ series.

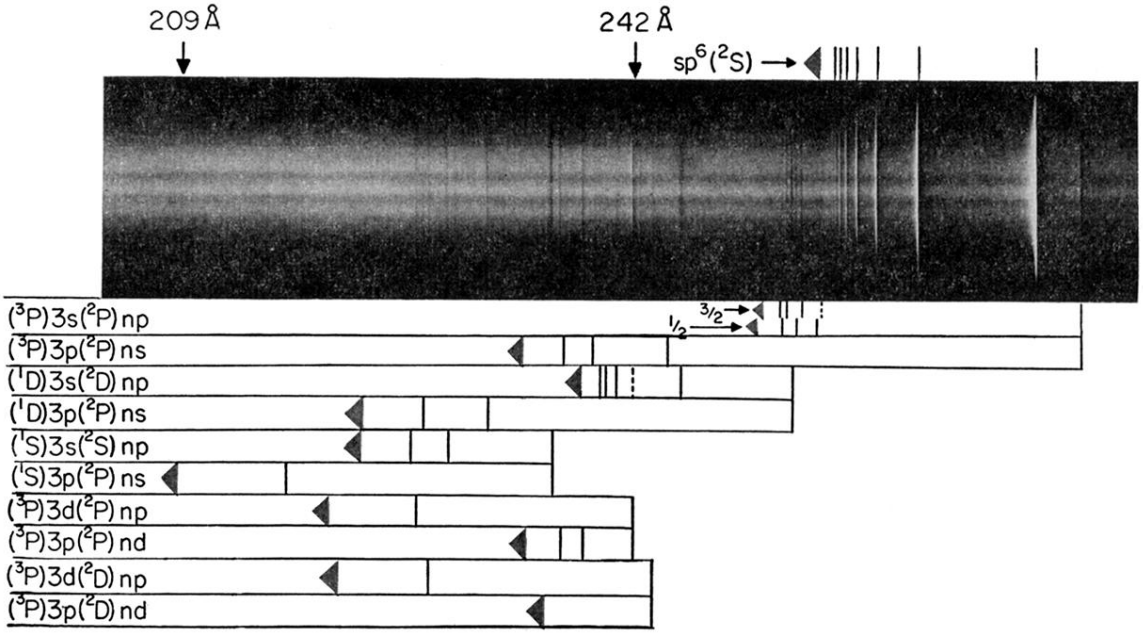

FIG. 3. The absorption spectrum of neon in the 200–280 Å region, showing (to the right) the strong asymmetric resonances due to the excitation of a subshell 2*s* electron. The remaining weaker structures are due to the simultaneous excitation of two 2*p* electrons. (The photograph is a positive print and therefore black denotes absorption.)